

# Plastic behavior of 304 stainless steel for complex loading at high temperature

K.Ikegami & Y.Niitsu

*Tokyo Institute of Technology, Yokohama, Japan*

## 1 INTRODUCTION

The structural components used at high temperature are subjected to the severe condition of combining complex loading and temperature history. For the strength design of such components, it is necessary to investigate the deformation behavior of materials used at high temperature. The high temperature deformation is correlated with loading condition and temperature state in complicated manner. Experimental investigations on the high temperature deformation are reported by several researchers. The results are summarized by the authors (Ikegami & Niitsu 1985b). Extensive and systematic experiments are necessary to understand the high temperature deformation. The authors continue experimental works on the plastic deformation at high temperature and report the results in the papers listed in the reference. This paper presents some characteristic behavior of metal at high temperature on the basis of the authors' experimental results.

## 2 EXPERIMENTAL METHOD

The experiments were conducted by subjecting thin-walled tubular specimens to combined axial load and torsion by a combined stress testing machine (Ikegami and Niitsu 1985a). The dimension of the specimen is given in Figure 1. The material of the specimen is an austenite stainless steel SUS 304. The chemical composition of this material as percentage by weight is indicated in Table 1. Before testing, the machined specimens were heat-treated in vacuum at 1050°C for one-half hour and then they were cooled in air out of vacuum chamber.

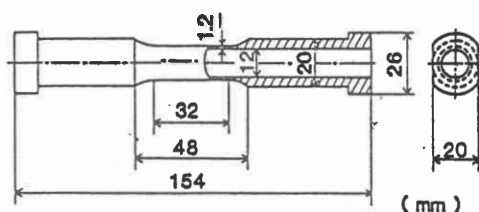


Figure 1. Shape and dimensions of the specimen.

Table 1. Chemical compositions of the testing materials.

C	Si	Mn	P	S	Ni	Cr	Fe
0.07	0.62	1.23	0.27	0.03	8.74	18.2	70.8

( Weight % )

The specimen was heated by a high frequency induction heating apparatus. The temperature of the specimen was measured by three P-PR thermocouples. Two measuring devices of lever type were used to obtain the axial and torsional strains of the specimen (Ikegami and Niitsu 1985a). The loading conditions were controlled with equivalent values of true stress at 0.653 MPa/sec on the loading path.

### 3 EXPERIMENTAL RESULTS AND DISCUSSIONS

#### 3.1 Effect of complex loading

Figure 2 shows the stress paths used in the experiments. The specimens were loaded to 3% of tensile plastic strain and then reloaded into different direction indicated in Figure 2. The testing temperatures are 27°C (room temperature), 200°C, 400°C and 600°C. The results at room temperature and 400°C are represented in tensile and shear stresses plane of Figure 3. The points in the figure are the stress points corresponding to defined values of equivalent plastic strain in reloading from the prestress point. The curves connecting the stress points having the same subsequent plastic strain values are defined as the equi-plastic strain surfaces (Ikegami & Niitsu 1985b). The surfaces are formulated by the following equations.

$$\frac{(\sigma - \sigma_*)^2}{\xi + \eta \operatorname{sgn}(\sigma - \sigma_*)} + \frac{3\tau^2}{(\sigma_F - \sigma_C)} - 1 = 0 \quad \dots\dots (1)$$

$$\xi = \{(\sigma_F - \sigma_*)^2 + (\sigma_* + \sigma_F - \sigma_B)^2\} / 2$$

$$\eta = \{(\sigma_F - \sigma_*)^2 - (\sigma_* + \sigma_F - \sigma_B)^2\} / 2$$

$$\operatorname{sgn}(x) = \begin{cases} 1 & x > 0 \\ 0 & x = 0 \\ -1 & x < 0 \end{cases}$$

The one surface determined by equation 1 is schematically illustrated in Figure 4. The curves of broken line is a circle with radius  $\sigma_F$ , where the notation  $\sigma_F$  is the flow stress in uniaxial tension. This circle is the reference to define the notations  $\sigma_F, \sigma_B, \sigma_C, \sigma_*$  in equation 1. The notation  $\sigma_B$  is a decrease of the flow stress in the opposite direction to the preloading,  $\sigma_C$  a decrease of the flow in the perpendicular direction to the preloading and  $\sigma_*$  a shift of the center of the curve. These values are correlated with the subsequent plastic strain  $\rho_2^P$  and the temperature T by the following equations.

The parameters in  $\sigma_F$  are given in Table 2.

$$\sigma_F = \sigma_y + H\rho^a$$

$$\sigma_B = \sigma_{B0} + \Delta\sigma_B$$

$$\sigma_{B0} = \sigma_1(-1.12 \times 10^{-4} T + 0.113) \times \{1 - \exp(-0.39\rho_1^P)\}$$

$$\Delta\sigma_B = (\sigma_1 - \sigma_{B0})\{1.80 \exp(-g\sqrt{\rho_2^P})\}$$

$$g = 5.31 + (1 - 9.85 \times 10^{-4} T)\{-2.26 + 2.37 \exp(-0.61\rho_1^P)\}$$

$$\sigma_B(600^\circ\text{C}) = \sigma_1\{1.61 \exp(-6.18\sqrt{\rho_2^P}) + 0.071\}$$

$$\sigma_C = 0.499\sigma_B \exp(-2.1\sqrt{\rho_2^P}) - \sigma_h$$

$$\sigma_* = 0.499\sigma_B \exp(-0.802\sqrt{\rho_2^P})$$

$$\sigma_1 = \sigma_F(\rho = \rho_1^P)$$

$$27 \leq T \leq 400(^\circ\text{C})$$

$$\sigma_h(\text{R. T., 3 \%}) = 26 \text{ MPa}$$

$$\sigma_h(200^\circ\text{C, 3 \%}) = 18 \text{ MPa}$$

$$\sigma_h(400^\circ\text{C, 3 \%}) = 20 \text{ MPa}$$

$$\sigma_h(600^\circ\text{C, 3 \%}) = 12 \text{ MPa}$$

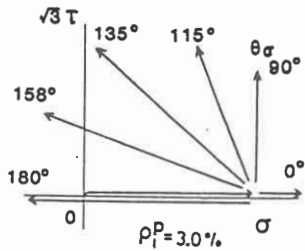


Figure 2. Stress path with a corner.

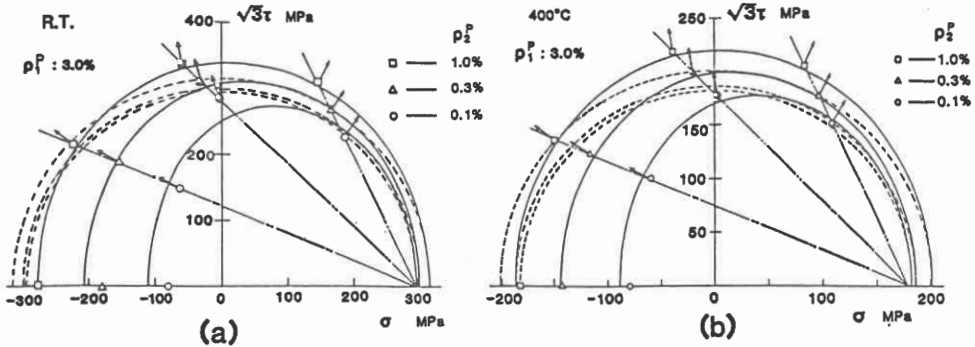


Figure 3. Equi-plastic strain surfaces subsequent to tensile prestraining

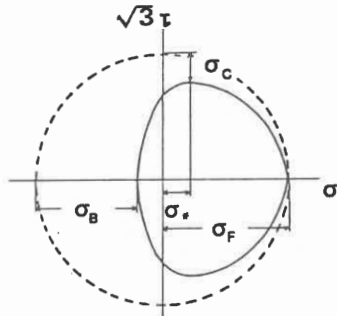


Figure 4. Schematic figure of the equi-plastic strain surface.

Table 2. Material constants for the stress strain relation.

Temp.	$\sigma_y$ MPa	H MPa	$\alpha$
27°C	189.8	48.7	0.69
200°C	112.8	34.9	0.80
400°C	93.3	36.5	0.78
600°C	72.1	37.1	0.76

The solid curves in Figure 3 are the subsequent equi-plastic strain surfaces calculated by equation 1. The curves of broken line are the equi-plastic strain surfaces for the initial state which are determined by proportional loadings. Comparing the equi-plastic strain surfaces of the subsequent state with those of the initial state, the expansion and translation of the surfaces by preloading are observed. The hardening in the transverse direction to preloading is remarkable. It seems that latent hardening is produced in the direction. The arrows in the curves are the directions of the plastic strain vectors at the stress points. The directions are normal to the curves. The plastic strain can be calculated by applying the flow rule to the equi-plastic strain surfaces.

Figure 5 shows the equivalent stress and plastic strain relations for the subsequent loading in Figure 2. The curves in the figure are

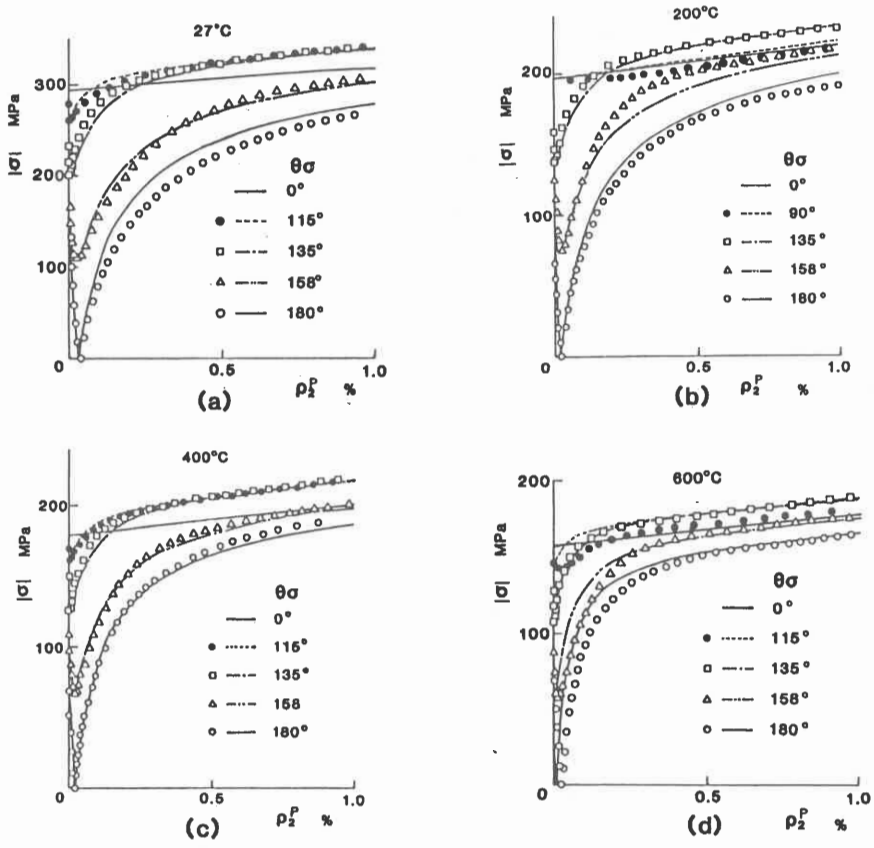


Figure 5. Equivalent stress strain curves subsequent to plastic prestraining.

calculated relations by using the equi-plastic strain surfaces. The flow stresses in the directions of 135° and 115° is larger than the flow stress in monotonic tensile loading. The hardening rate to the flow stress becomes the maximum at 400°C.

### 3.2 Effect temperature history

The tensile loading test was conducted under the condition of changing temperature in the range of room temperature to 600°C. The loading and temperature conditions are shown in Figure 6. The testing temperature was changed by the rate of about 2.0°C/sec in partial unloaded state and held before loading for 5 minutes. Figure 7 shows the obtained tensile stress strain relation. The marks are the experimental results and the chain curves are the tensile stress strain curves under constant temperatures. The strain is indicated by the plastic strain minus thermal strain. The stress strain relations under variable temperatures coincide with the relations under constant temperature. The flow stress does not depend on the temperature history but depends on the accumulated plastic strain for monotonic loading.

The plastic behavior subsequent on tensile prestrain was investigated at variable temperature state. The loading conditions are shown in Figure 8. The tensile loading is given at room

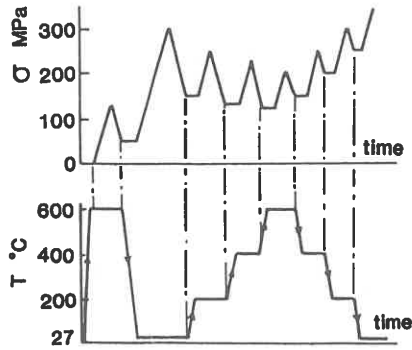


Figure 6. Loading condition under variable temperatures.

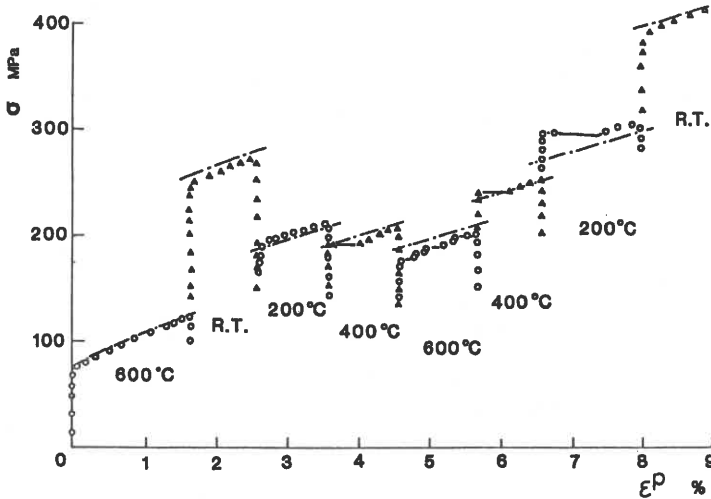


Figure 7. Stress strain relations under variable temperatures.

temperature or at 600°C and then the temperature of the specimen was changed to 600°C or room temperature. The subsequent combined loading was conducted into various directions of  $\theta_{\sigma} = 0^{\circ}, 90^{\circ}, 135^{\circ}, 158^{\circ}$  and  $180^{\circ}$ .

The equi-plastic strain surfaces for the subsequent plastic strain of 0.05%, 0.2% and 1.0% are represented with the curves of solid line in Figure 9. The curves are the calculated results by using equation 1. The experimental stress points in the equi-plastic strain surfaces at 600°C agree with the calculated curves. But the discrepancy between calculated and experimental results at room temperature becomes large in the opposite direction to prestraining.

The curves of broken line are the equi-plastic strain surfaces at 600°C in Figure 9(a) and at room temperature in Figure 9(b), respectively. The equi-plastic strain surfaces determined at 600°C subsequent to prestraining at room temperature contracts with the retreat of the surfaces at room temperature. But the surfaces determined at room temperature subsequent to prestraining at 600°C expands with the translation of the surfaces at 600°C.

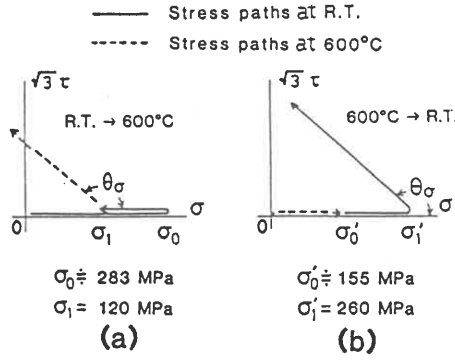


Figure 8. Subsequent loading paths under variable temperatures.

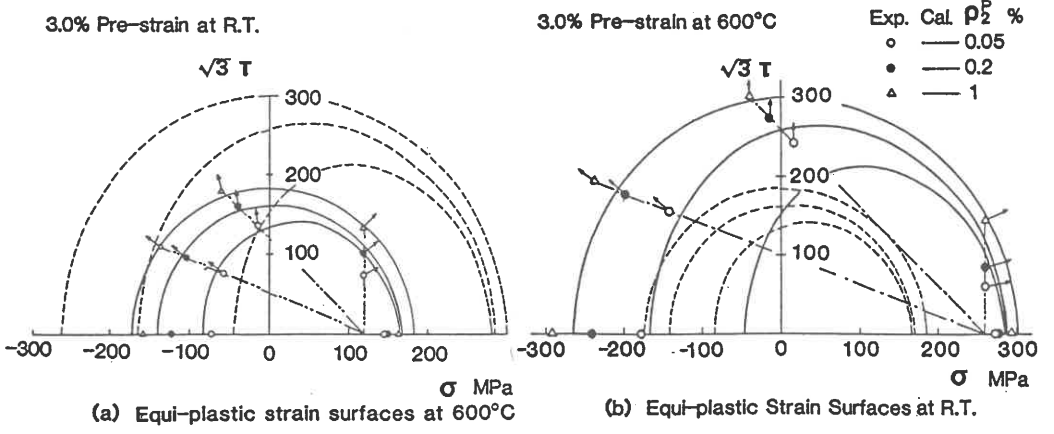


Figure 9. Equi-plastic strain surfaces subsequent to plastic prestraining under variable temperatures.

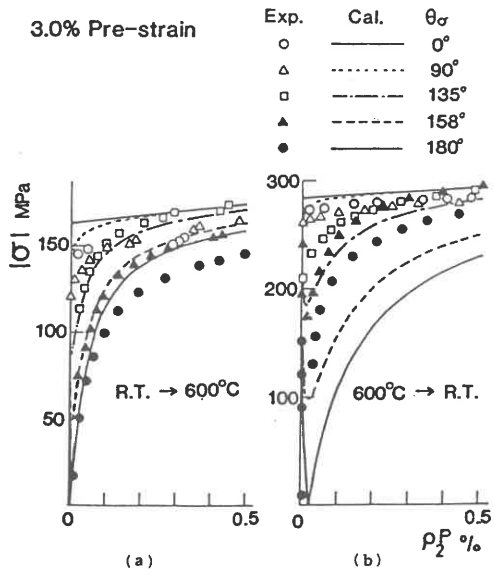


Figure 10. Equivalent stress strain curves subsequent to plastic straining under variable temperatures.

Figure 10 shows the equivalent stress strain relations for the subsequent loading of Figure 8. The curves are calculated by using equation 1 and flow rule on the assumption of neglecting temperature history. The calculated results at 600°C coincide with the experimental results. In the results at room temperature, the calculated curves does not fit for the experimental result in the opposite side to the prestraining direction. This means that the effect of temperature history is remarkable in Bauschinger curves for the case of falling temperature.

### 3.3 Effect of creep prestrain

The monotonic loading tests including creep straining were conducted by tensile test or torsional test at room temperature, 400°C and 600°C. The equivalent stress and inelastic strain curves are shown in Figure 11. The solid, broken and chain curves are the stress and plastic strain relations under constant temperature. The holding time for creep straining and the magnitude are indicated by the dashed lines in the figure. At room temperature, the plastic strain subsequent to creep prestraining was not produced until the increasing stress approached the solid curve. After the stress reached the solid curve, the plastic strain was produced again and the flow stress coincided with the solid curve. This tendency is observed both in tensile and torsional loading tests. This means that creep strain has the same hardening effect as plastic strain at room temperature. In the results at 600°C, the similar hardening tendency by creep strain is observed, but the magnitude is small comparing with the hardening by plastic strain. The creep strain at 400°C was produced in small magnitude and the hardening effect was not confirmed.

The subsequent combined loading tests were conducted after creep straining under constant temperature. The stress paths used in the experiments are shown in Figure 12. The specimens were loaded into plastic range by tension and the stress to the specimens was held at 250 MPa for about 6 hours at room temperature or at 154 MPa for about 24 hours. With those preloading processes, the plastic and creep prestrains ( $\rho_1^p$  and  $\rho_1^c$ ) were given to the specimens. The values of plastic and creep strains were 1.4% and 1.6% at room temperature, and 2.6% and 1.2% at high temperature, respectively. The subsequent loading were conducted into various directions of the angle  $\theta_\sigma$  from the prestress points. The loading directions were chosen as  $\theta_\sigma = 0^\circ$ ,

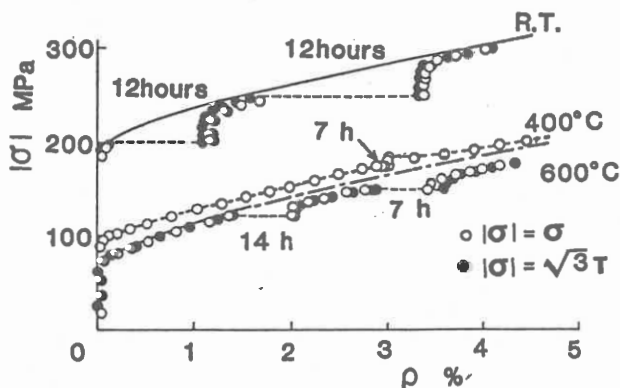


Figure 11. Equivalent stress strain curves including creep strain.

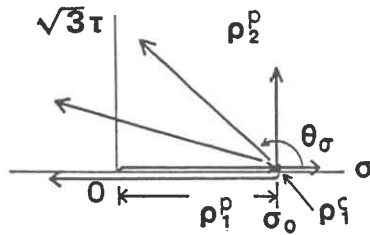


Figure 12. Stress paths with creep straining.

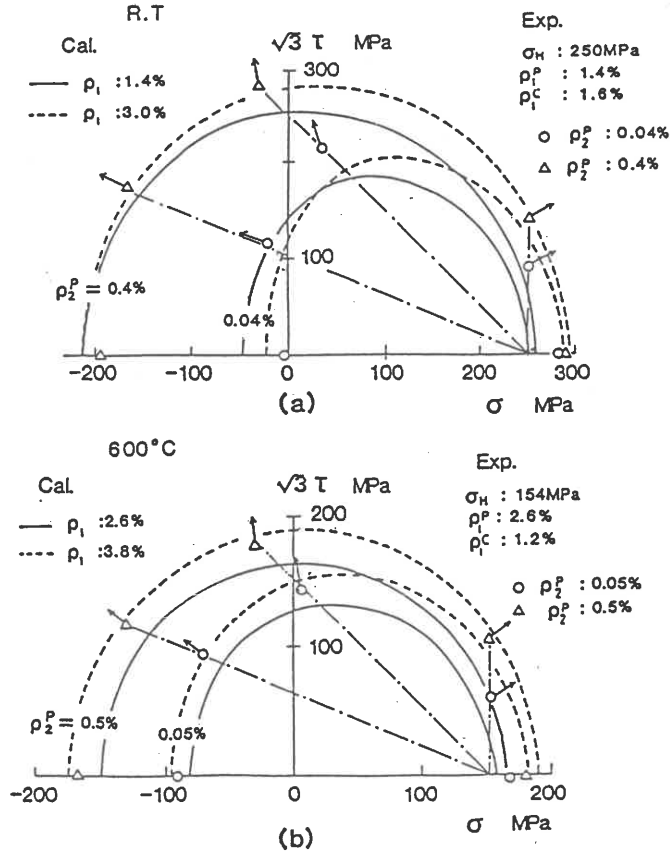


Figure 13. Equi-plastic strain surfaces subsequent to plastic and creep strainings.

90°, 135°, 158° and 180°. The plastic behavior subsequent to plastic and creep prestraining is compared with the equi-plastic strain surfaces in Figure 13. The curves of solid line are the surfaces calculated by using equation 1 on the assumption of neglecting the hardening effect of creep strain. The curves of broken line are the results of including the hardening by creep strain on the assumption of equivalent hardening effect between plastic and creep deformation.

At room temperature, the subsequent stress points coincide with the curves of broken line. The hardening effect of creep strain is nearly equal to that of plastic strain in combined stress state. The experimental stress points at 600°C are close to the broken curves or

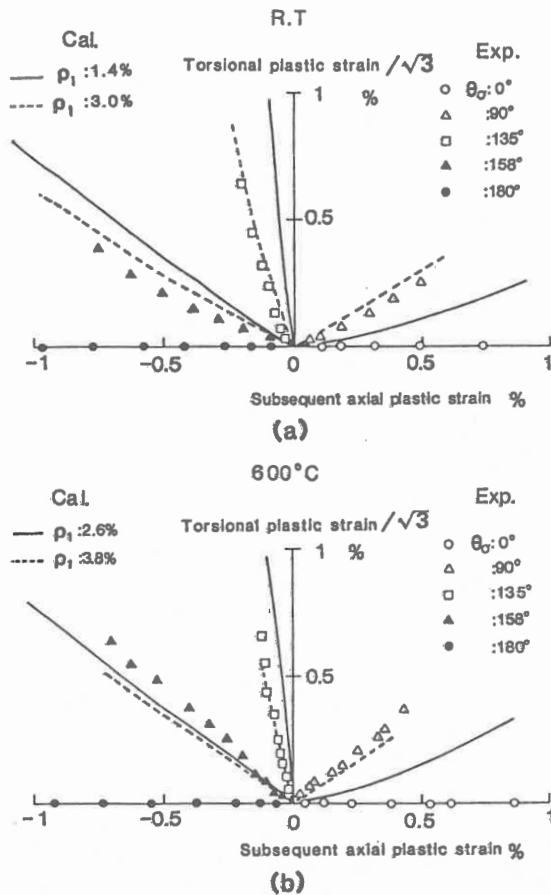


Figure 14. Plastic strain trajectories subsequent to plastic and creep strainings.

between the broken and solid curves. The hardening effect due to creep strain at high temperature is slightly weaker than that of plastic strain. Comparing two curves illustrated by solid and broken lines in Figure 13, it is found that the hardening mode by creep strain at room temperature is similar to kinematic hardening and, at high temperature, the mode resembles to isotropic hardening.

Figure 14 is the comparison of the strain trajectories corresponding to the results of Figure 13. The solid and broken lines are the trajectories calculated by applying the flow rule to the equi-plastic strain surfaces. The results indicated with the solid and broken lines are respectively obtained on the assumption of neglecting and including the hardening effect by creep strain with above mentioned way. The experimental trajectories both at room temperature and 600°C are close to the results of broken line. The plastic hardening is produced by creep strain.

### 3.4 Effect of cyclic loading

The stress strain curves in cyclic loading by tension and compression were obtained under various temperature conditions. The cyclic

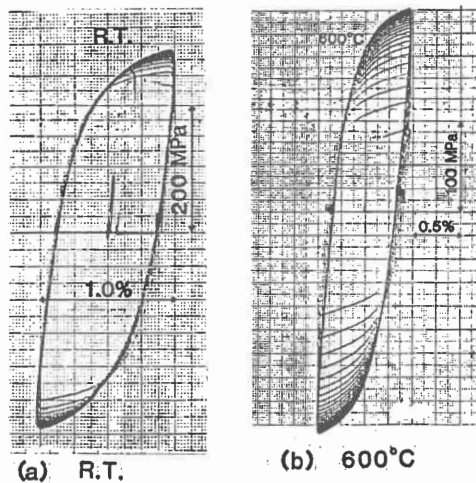


Figure 15. Cyclic stress strain curves at constant temperature.

loading was performed between fixed strain amplitude. Figure 15 shows the cyclic stress strain curves under the strain amplitude of 1.0% for 20 cycles at room temperature and for 30 cycles at 600°C. The maximum tensile stress in cyclic stress strain curves at room temperature varies from 230 MPa in the initial cycle to 295 MPa in 20 cycles. The flow stress at room temperature exhibits the increase of 30% by cyclic loading. In the cyclic stress strain curves at 600°C, the flow stress increases by 150% during 20 cycles. The hardening properties in cyclic loading depends strongly on the temperature state.

Figure 16 shows the cyclic hardening behavior during 20 cycles with the strain amplitude of 1.0% under the condition of changing temperature between room temperature and 200°C or between room temperature and 600°C. The sequence of testing temperature is the cyclic change of room temperature and high temperature. In the cyclic test between room temperature and 200°C, the maximum flow stress is about 300 MPa in the second and third cyclic loading at room temperature. The value is equal to the maximum flow stress in the initial cyclic loading. But the maximum flow stress of cyclic loading between room temperature and 600°C becomes 400 MPa in the second and third cyclic loading in room temperature. The effect of temperature history is observed on the saturation properties of cyclic hardening.

Figure 17 shows the variation of the maximum stress in cyclic loading at different temperature conditions. In the tests between room temperature and 200°C of Figure 17(a), the maximum stress after the second cyclic loading at room temperature and 200°C is nearly constant. In Figure 17(b), the maximum stresses at room temperature and 600°C are varied by cyclic loading. The increase of the maximum stress in the first cyclic loading is remarkable at 600°C. The maximum stress increases also in the second and third cyclic loadings. But, in the cyclic loading at room temperature, the maximum stress decreases during cyclic loading, though the initial maximum stress in each cyclic loading process increases comparing with the final maximum stress in the previous cyclic loading at room temperature. The results of Figure 17(c) shows similar tendency to Figure 17(b). The variation of the maximum stress of Figure 17(d) is different from the results of Figures 17(a) to (c). The softening by decrease of the maximum stress is not observed and the cyclic hardening is produced in each cyclic loading process at both temperature conditions of 400°C and 600°C.

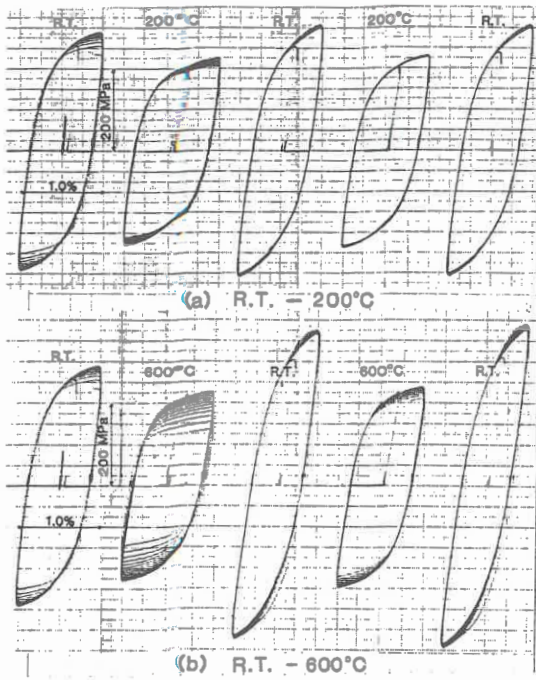
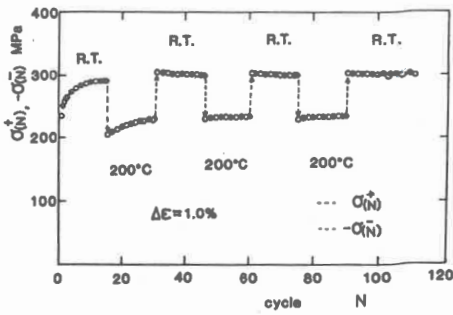
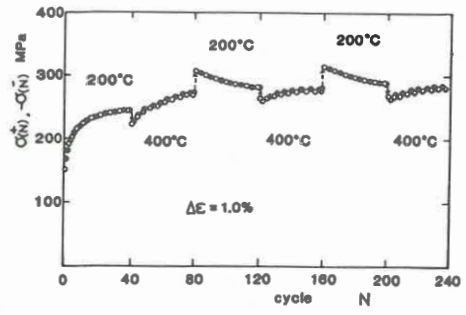


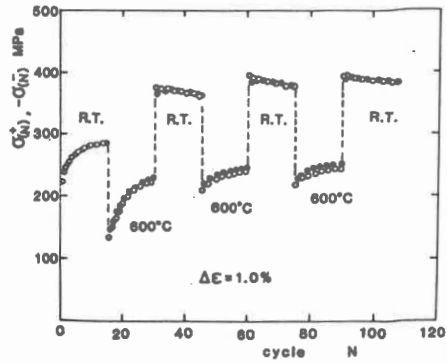
Figure 16. Cyclic stress strain curves under variable temperatures.



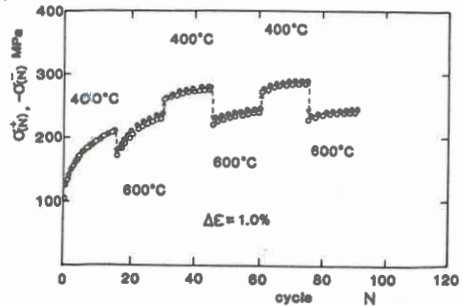
(a)



(c)



(b)



(d)

Figure 17. Effects of temperature history on the maximum cyclic stress.

#### 4 SUMMARY AND CONCLUSIONS

The stress strain relations in plastic range of 304 stainless steel were experimentally investigated at high temperature by subjecting thin-walled tubular specimens to combined axial load and torsion. The effect of plastic prestraining, temperature history, creep prestraining and cyclic loading were examined on the equivalent stress strain curves and the equi-plastic strain surfaces under various loading conditions. The equi-plastic strain surfaces were defined by the locus of stress points having the equivalent plastic strain hardening magnitude under combined stress state. The obtained results are summarized as follows.

1) The equi-plastic strain surfaces were deformed into egg-shape by prestraining. The hardening is remarkable in the transverse direction to prestraining.

2) The effect of temperature history on flow stress was small for monotonic loading, but the effect was observed in the stress strain relations in reverse loading.

3) The creep strain had the same hardening effect as the plastic strain at room temperature. But the effect of creep strain on plastic hardening was weak comparing with the hardening by plastic strain.

4) The cyclic hardening was more remarkable at high temperature than in room temperature. The coupled effect between loading and temperature conditions was found in cyclic hardening at variable temperatures.

#### REFERENCES

- Niitsu, Y., K. Ikegami & E. Shiratori 1984a. Bull. JSME. 230: 1585-1591.  
Niitsu, Y., K. Ikegami 1984b. Bull. JSME. 233: 2332-2338.  
Niitsu, Y., K. Ikegami 1984c. Trans. Japan Soc. Mech. Engrs. 453A: 996-1002. (in Japanese)  
Ikegami, K., Y. Niitsu 1985a. Eng. Fracture Mech. 21: 897-907.  
Ikegami, K., Y. Niitsu 1985b. Int. J. Plasticity. 1: 331-345.  
Niitsu, Y., K. Ikegami 1985c. Bull. JSME. 243: 1853-1858.  
Niitsu, Y., K. Ikegami 1985d. Bull. JSME. 246: 2853-2858.  
Niitsu, Y., D. Tsuji & K. Ikegami 1986a. Trans. Japan Soc. Mech. Engrs. 474A: 486-492 (in Japanese)  
Niitsu, Y., K. Ikegami 1986b. Trans. Japan Soc. Mech. Engrs. 478A: 1621-1627. (in Japanese)